Experimental and Theoretical Study of the Kinetic and Thermodynamic Sites of Protonation in $(CO)Pt(\mu\text{-}PBu^t_2)_2Pt(PBu^t_2H)$

Piero Leoni,*,†,‡ Marco Pasquali,† Valerio Cittadini,† Alessandro Fortunelli,§ and Massimo Selmi§

Dipartimento di Chimica e Chimica Industriale dell'Università di Pisa and Istituto di Chimica Quantistica ed Energetica Molecolare (ICQEM) del CNR, Via Risorgimento 35, I-56126 Pisa, Italy, and Scuola Normale Superiore, Piazza dei Cavalieri 7, I-56126 Pisa, Italy

Received March 22, 1999

The Pt^IPt^I monocarbonyl derivative $(Bu^t_2HP)Pt(\mu\text{-}PBu^t_2)_2Pt(CO)$ (**5**), with a planar, asymmetrically substituted $Pt_2(\mu\text{-}PBu^t_2)_2$ core, reacts with CF_3SO_3H to give the new $Pt^{II}Pt^{II}$ carbonyl hydride $[(Bu^t_2HP)Pt(\mu\text{-}PBu^t_2)_2Pt(CO)(H)]CF_3SO_3$ (**6a**). Complex **6a**, in which the proton is terminally attached to the Pt atom bearing the carbonyl ligand, is formed under kinetic control and is stable in well-dried nonbasic solvents. This isomer is converted quantitatively by an external weak base into the thermodynamically favored form, $[(PBu^t_2H)(H)Pt(\mu\text{-}PBu^t_2)_2Pt(CO)]CF_3SO_3$ (**6b**), in which the proton is terminally attached to the Pt atom bearing the phosphine group. In the presence of an excess of triflic acid, **6a** is further protonated to give $[Pt_2(\mu\text{-}PBu^t_2)(\mu\text{-}H)(CO)(PBu^t_2H)(\eta^2\text{-}PBu^t_2H)](CF_3SO_3)_2$ (**7**) by the formation of a P−H bond between the hydride and the adjacent phosphido ligand induced by metal protonation. Complex **7** was characterized by multinuclear NMR spectroscopy, which strongly suggests a Pt−H−P agostic interaction. Like **6a**, complex **7** is stable in nonbasic media, but yields **6b** rapidly and quantitatively in the presence of a base. Experimental data compare well with the results of ab initio calculations on model compounds corresponding to **5**, $\mathbf{6a}^+$, and $\mathbf{6b}^+$, whose structures have been optimized in the gas phase.

Introduction

The rates of proton transfer processes involving transition metals are known to be considerably slower than those centered on hard (mainly N and O) sites and comparable to those centered on carbon bases.[1−4] This is generally attributed to the less favorable preassociation of hydrogen-bonded pairs[3] and to the major electronic and structural reorganization implied by the metal- (or carbon-) centered reactions.[1−5] Steric hindrance, another factor which influences the rate of proton transfer, [6−8] again disfavors metal (or carbon) bases compared to hard bases.

The protonation at the metal can be in competition with the protonation at other basic sites of the complex, and the overall reaction can proceed through the formation of intermediate kinetic species.[1−4]Alternative basic sites were shown to be carbon,[3,9−17] nitrogen,[18] oxygen,[19−24] sulfur,[25,26] halide,[4,27,28] or hydride[1,29−34] ligands. As a rough approximation, hard ligands are protonated faster than the metal, provided they have free lone pairs not involved in π-interactions.[2,35,36]

In polynuclear systems, a competition for the proton between

† Università di Pisa.
‡ Scuola Normale Superiore.
§ ICQEM.

(1) Kristjánsdóttir, S. S.; Norton, J. R. In *Transition Metal Hydrides*; Dedieu, A., Ed.; VCH Publishers: New York, 1992; Chapter 9.
(2) Kramarz, K. W.; Norton, J. R. *Prog. Inorg. Chem.* **1994**, *42*, 1.
(3) Henderson, R. A. *Angew. Chem., Int. Ed. Engl.* **1996**, *31*, 947.
(4) Kuhlman, R. *Coord. Chem. Rev.* **1997**, *167*, 205.
(5) Walker, H. W.; Kresge, C. T.; Ford, P. C.; Pearson, R. G. *J. Am. Chem. Soc.* **1979**, *101*, 7428.
(6) Darensbourg, M. Y.; Ludwig, M. M. *Inorg. Chem.* **1986**, *25*, 289
(7) Ryan, O. B.; Tilset, M. *J. Am. Chem. Soc.* **1991**, *113*, 9554.
(8) Smith, K.-T.; Romming, C.; Tilset, M. *J. Am. Chem. Soc.* **1993**, *115*, 8681.
(9) Crocco, G. L.; Gladysz, J. A. *J. Am. Chem. Soc.* **1988**, *110*, 6110.
(10) Osborn, V. A.; Parker, C. A.; Winter, M. J. *J. Chem. Soc., Chem. Commun.* **1986**, 1185.
(11) Carvalho, M. F. N. N.; Henderson, R. A.; Pombeiro, A. J. L.; Richards, R. L. *J. Chem. Soc., Chem. Commun.* **1989**, 1796.
(12) Oglieve, K. E.; Henderson, R. A. *J. Chem. Soc., Chem. Commun.* **1993**, 474.
(13) Henderson, R. A.; Oglieve, K. E. *J. Chem. Soc., Dalton Trans.* **1996**, 3397.
(14) Oglieve, K. E.; Henderson, R. A. *J. Chem. Soc., Dalton Trans.* **1991**, 3295.
(15) Heinekey, D. M.; Michel, S. T.; Schulte, G. K. *Organometallics* **1989**, *8*, 1241.
(16) Herrmann, W. A.; Plank, J.; Ziegler, M. L.; Balbach, B. *J. Am. Chem. Soc.* **1980**, *102*, 5906.
(17) Spencer, J. L.; Mhinzi, G. S. *J. Chem. Soc., Dalton Trans.* **1995**, 3819.
(18) Bianchini, C.; Laschi, F.; Orraviani, M. F.; Peruzzini, M.; Zanello, P.; Zanobini, F. *Organometallics* **1989**, *8*, 893.
(19) Whitmire, K. H.; Shriver, D. F. *J. Am. Chem. Soc.* **1981**, *103*, 6754.
(20) Nevinger, L. R.; Keister, J. B.; Maher, J. *Organometallics* **1990**, *9*, 1900.
(21) Rosenberg, E. *Polyhedron* **1989**, *8*, 383.
(22) Stevens, R. E.; Guettler, R. D.; Gladfelter, W. L. *Inorg. Chem.* **1990**, *29*, 451.
(23) Hash, K. R.; Rosenberg, E. *Organometallics* **1997**, *16*, 3593.
(24) Driver, M. S.; Hartwig, J. F. *Organometallics* **1997**, *16*, 5706.
(25) Darensbourg, M. Y.; Liaw, W.-F.; Riordan, C. G. *J. Am. Chem. Soc.* **1989**, *111*, 8051.
(26) Grönberg, K. L. C.; Henderson, R. A. *J. Chem. Soc., Dalton Trans.* **1996**, 3667.
(27) Patel, B. P.; Crabtree, R. H. *J. Am. Chem. Soc.* **1996**, *118*, 13105.
(28) Kuhlman, R.; Streib, W. E.; Huffman, J. C.; Caulton, K. G. *J. Am. Chem. Soc.* **1996**, *118*, 6934.
(29) Chinn, M. S.; Heinekey, D. M. *J. Am. Chem. Soc.* **1990**, *112*, 5166.
(30) Jia, G.; Lough, A. J.; Morris, R. H. *Organometallics* **1992**, *11*, 161.
(31) Parkin, G.; Bercaw, J. E. *J. Chem. Soc., Chem. Commun.* **1989**, 255.
(32) Bullock, R. M.; Song, J.-S.; Szalda, D. J. *Organometallics* **1996**, *15*, 2504.
(33) Hamon, P.; Toupet, L.; Hamon, J.-P.; Lapinte, C. *Organometallics* **1992**, *11*, 1429.
(34) Henderson, R. A.; Oglieve, K. E. *J. Chem. Soc., Dalton Trans.* **1993**, 3431.
(35) Carrol, J. M.; Norton, J. R. *J. Am. Chem. Soc.* **1992**, *114*, 8744.

10.1021/ic9903228 CCC: $18.00
Published on Web 10/22/1999

Scheme 1

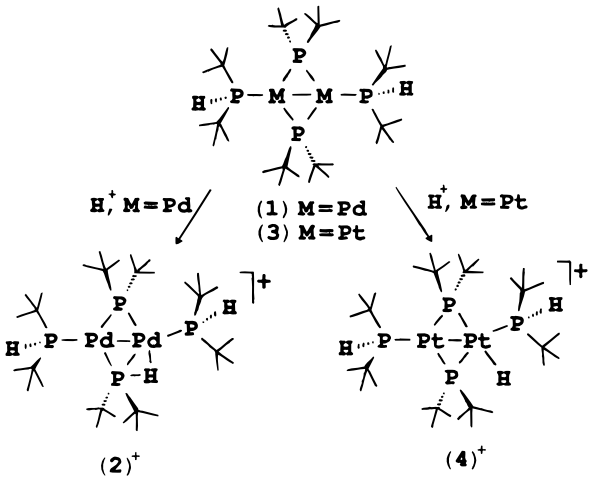

different basic sites can be observed;[1] moreover, proton transfers to and from a terminal hydride were found to be faster than those involving bridging hydrides.[37,38]

As we have previously shown, the Pd_2^I complex [Pd(μ-PBu^t_2)(PBu^t_2H)]$_2$ (**1**)[39] is protonated by CF_3SO_3H at one of the Pd−P_μ bonds to give the Pd_2^I derivative [Pd_2(μ-PBu^t_2)(μ-PBu^t_2H)(PBu^t_2H)$_2$]CF_3SO_3 (**2**), with a Pd−H−P agostic bond.[40] The same reaction performed on the platinum analogue of **1**, [Pt(μ-PBu^t_2)(PBu^t_2H)]$_2$ (**3**),[41] was instead found to give the classical Pt_2^{II} hydride [(Bu^t_2HP)Pt(μ-PBu^t_2)$_2$Pt(H)(PBu^t_2H)]CF_3SO_3 (**4**)[42] (Scheme 1).

We report here an experimental and theoretical investigation of the reaction of (Bu^t_2HP)Pt(μ-PBu^t_2)$_2$Pt(CO) (**5**)[41] with triflic acid, which proceeds through the initial protonation of the less hindered metal, and the isomerization of the kinetic hydride to its thermodynamic isomer.

Results and Discussion

A red CH_2Cl_2 solution of **5** turned immediately yellow when reacted with 1 equiv of CF_3SO_3H. Rapid workup of the reaction mixture afforded [(Bu^t_2HP)Pt(μ-PBu^t_2)$_2$Pt(CO)(H)]CF_3SO_3 (**6a**) as a yellow powder in ca. 60% yield (Scheme 2).

Three groups of resonances were observed in the $^{31}P\{^1H\}$ NMR spectrum of **6a** at 62.1 (P_3), 342.5 (P_1), and 393.5 (P_2) ppm. The very low field position of the resonances assigned to P_1 and P_2 suggests the presence of a metal−metal bond, in agreement with the results of a theoretical study on the strictly related cation $\mathbf{4}^+$.[42] Owing to the isotopic abundance (33.8%) of ^{195}Pt, the spectrum is the sum of four subspectra (the composition of the isotopomers, the NMR parameters of **6a**, **6b**, and **4**, and the numbering scheme used in the following discussion are shown in Table 1).

Scheme 2

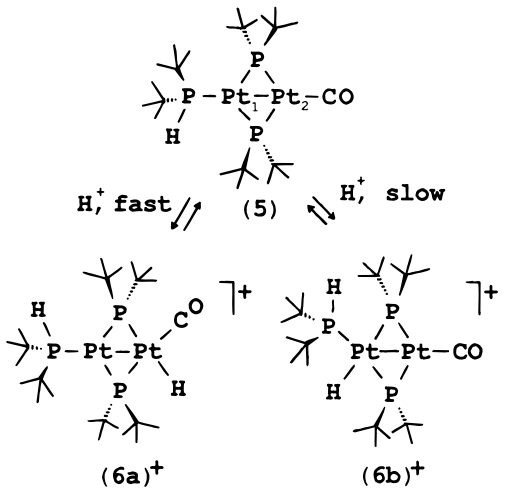

Table 1. ^1H, ^{31}P, and ^{195}Pt NMR Parameters for Cations **6a**$^+$ (Top), **6b**$^+$ (Middle), and **4**$^+$ (Bottom)

	P_1	P_2	P_3	P_4	Pt_1	Pt_2	H_1
P_1	342.5	228	42	-	2472	1273	10
	338.8	153	-	116	2855	833	14
	329.5	212	63	132	2888	934	14
P_2		393.5	31	-	2595	961	80
		369.0	-	8.5	2202	1484	99
		348.0	21	10	2090	1643	109
P_3			62.1	-	4672	183	10
			-	-	-	-	-
			57.5	37	4762	87	5.5
P_4				-	-	-	-
				30.5	-	2918	25.5
				30.3	-	3034	28.5
Pt_1					-5486	617	-
					-5299	390	-
					-5586	340	-
Pt_2						-5936	679
						-6163	683
						-6268	690
H_1							-1.5
							-2.6
							-3.4

Isotop	Pt_1	Pt_2	%
A	-	-	43.8
B	195	-	22.4
C	-	195	22.4
D	195	195	11.4

cation	L_3	L_4
(6a)+	PBu^t_2H	CO
(6b)+	CO	PBu^t_2H
(4)+	PBu^t_2H	PBu^t_2H

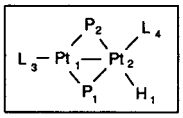

The central lines of each signal (isotopomer **A**) are doublets of doublets. As usually observed in derivatives containing a M_2(μ-PR_2)$_2$ (M = Pd, Pt) planar core,[41−46] the bridging P nuclei are strongly mutually coupled ($^2J_{P1P2}$ = 228 Hz). Moreover, similar values were found for $^2J_{P3P1}$ (42 Hz) and $^2J_{P3P2}$ (31 Hz), thus suggesting a trigonal-planar geometry for the platinum bonded to the terminal PBu^t_2H molecule. This is confirmed by the large value of $^1J_{P3Pt1}$ = 4672 Hz [4762 Hz in **4** and 4438 and 4188 Hz in Pt(PPh_3)$_3$[47] and Pt(PEt_3)$_3$,[48] respectively]. Other values of PPt coupling constants from the ^{195}Pt satellites are given in Table 1.

The ^1H NMR spectrum shows a doublet ($^2J_{H1P2}$ = 80 Hz) of triplets ($^2J_{H1P1} \cong {}^3J_{H1P3}$ = 10 Hz) at −1.5 ppm for the terminal hydride ($^1J_{H1Pt2}$ = 679 Hz from ^{195}Pt satellites) and a doublet ($^1J_{P3H3}$ = 368 Hz) of triplets ($^3J_{P1H3} \cong {}^3J_{P2H3}$ = 13 Hz) at 6.4 ppm for the P−H proton of the secondary phosphine.

(36) Henderson, R. A.; Morgan, S. A.; Stephens, A. N. *J. Chem. Soc., Dalton Trans.* **1990**, 1101.
(37) Powell, J.; Sawjer, J. F.; Smith, S. J. *J. Chem. Soc., Dalton Trans.* **1992**, 2793.
(38) Powell, J.; Sawjer, J. F.; Stainer, M. V. R. *J. Chem. Soc., Chem. Commun.* **1985**, 1314.
(39) Leoni, P.; Sommovigo, M.; Pasquali, M.; Sabatino, P.; Braga, D. *J. Organomet. Chem.* **1992**, *423*, 263.
(40) Leoni, P.; Pasquali, M.; Sommovigo, M.; Laschi, F.; Zanello, P.; Albinati, A.; Lianza, F.; Pregosin, P. S.; Ruegger, H. *Organometallics* **1993**, *12*, 1702.
(41) Leoni, P.; Chiaradonna, G.; Pasquali, M.; Marchetti, F. *Inorg. Chem.* **1999**, *38*, 253.
(42) Leoni, P.; Pasquali, M.; Fortunelli, A.; Germano, G.; Albinati, A. *J. Am. Chem. Soc.* **1998**, *120*, 9564.
(43) Kourkine, I. V.; Chapman, M. B.; Glueck, D. S.; Eichele, K.; Wasylishen, R. E.; Yap, G. P. A.; Liable-Sands, L. M.; Rheingold, A. L. *Inorg. Chem.* **1996**, *35*, 1478.
(44) Alonso, E.; Fornies, J.; Fortuño, C.; Tomás *J. Chem. Soc., Dalton Trans.* **1995**, 3777.
(45) Brandon, J. B.; Dixon, K. R. *Can. J. Chem.* **1981**, *59*, 1188.
(46) Dawoodi, Z.; Eaborn, C.; Pidcock, A. *J. Organomet. Chem.* **1979**, *170*, 95.
(47) Leu, A.; Halpern, J. *Inorg. Chem.* **1980**, *19*, 1073.
(48) Mann, B. E.; Musco, A. *J. Chem. Soc., Dalton Trans.* **1980**, 776.

Table 2. Interatomic Separations[a]

	Pt_1-Pt_2	Pt_1-P_1	Pt_1-P_2	Pt_2-P_1	Pt_2-P_2	$Pt-P_{term}$	Pt−C	C−O	Pt_2-H_1	$P_1\cdots H_1$
5 (exp)	2.613	2.315	2.300	2.311	2.322	2.256	1.841	1.121		
5 (HF)	2.647	2.371	2.352	2.391	2.386	2.322	1.951	1.121		
5 (BLYP)	2.723	2.392	2.381	2.425	2.421	2.297	1.893	1.174		
5 (B3LYP)	2.692	2.368	2.357	2.400	2.394	2.284	1.889	1.158		
6a$^+$ (B3LYP)	2.792	2.298	2.295	2.397	2.592	2.280	1.941	1.141	1.610	2.615
6b$^+$ (B3LYP)	2.754	2.324	2.324	2.387	2.456	2.343	1.895	1.147	1.622	2.576

[a] The most relevant interatomic distances are reported as derived from experiment (exp) and theoretical calculations using the HF and two DF approaches (BLYP and B3LYP, respectively). Atom numbering is the same used in the discussion of NMR spectra; P_{term} is the phosphorus of the PBu$^t_2$H molecule; in complex **5**, Pt_1 is bonded to P_{term} and Pt_2 to CO. All the distances are given in Å.

The ^{195}Pt{^{1}H} NMR spectrum gives two signals at −5486 (ddd, Pt_1) and −5936 (ddd, Pt_2) ppm with weak satellites (isotopomer **D**, $^1J_{Pt1Pt2}$ = 617 Hz). The signal at −5936 ppm splits further in the proton-coupled spectrum due to the coupling with the terminal hydride. Significant absorptions in the IR (Nujol, KBr) spectrum were found at 2335 w (ν_{PH}), 2095 s (ν_{CO}), and 2043 w (ν_{PtH}) cm^{-1}.

When complex **6a** was dissolved in DME or acetone, a relatively fast ($\tau_{1/2}$ ca. 3 h) isomerization occurred to afford [(Bu$^t_2$HP)(H)Pt(μ-PBu$^t_2$)$_2$Pt(CO)]CF$_3$SO$_3$ (**6b**), in which the hydride ligand has moved to the phosphine-bearing platinum center. The appearance of the ^{31}P{^{1}H} NMR spectrum is similar to the one discussed above for **6a**, but significant differences were observed between the values of chemical shifts and coupling constants (see Table 1). An upfield shift is observed in the signal for the PBu$^t_2$H molecule (δ_{P4} = 30.5 ppm), which ends up close to the signal previously observed for the phosphine molecule cis to the hydride ligand in **4** (30.3 ppm). The bridging P nuclei resonate at 338.8 (P_1) and 369.0 (P_2) ppm. Conforming to structure **6b**, P_4 couples to the bridging nuclei with a large J_{trans} ($^2J_{P1P4}$ = 116 Hz) and a small J_{cis} ($^2J_{P2P4}$ = 8.5 Hz) value. The coupling of P_4 to the nearby tetracoordinated platinum center ($^1J_{P4Pt2}$ = 2918 Hz) is similar to the corresponding coupling in **4** (3034 Hz) and smaller than the coupling to a tricoordinated platinum ($^1J_{P3Pt1}$ = 4672 in **6a** and 4762 Hz in **4**). Other parameters from the spectra are similar to the corresponding parameters given by **6a** and **4** and will not be discussed further except the value of δ_H for the hydride ligand. This was found at −2.6 ppm, intermediate between the positions of the corresponding signals for **4** (−3.4 ppm) and **6a** (−1.5 ppm). Although H_1 should be considered a real hydride in both **6a** and **6b** [compare the small values of J_{H1P1} (<15 Hz, Table 2) with the corresponding value (151 Hz) found for the agostic palladium derivative **2**], a tempting explanation of this trend is that the value of δ_{H1} moves downfield as H_1 moves toward P_1. In this connection, we recall that δ_{H1} is at −0.16 ppm in the agostic **2**$^+$. Among others, another trend in Table 1 aligns similarly the three cations (**4**$^+$−**6b**$^+$−**6a**$^+$) and *could* be related to the approach of H_1 to P_1. This is the difference ($\Delta\delta_{P2,1}$) between the values of δ_{P2} and δ_{P1}, which was found at 18.5, 30.2 and 51.0 ppm, respectively, in **4**$^+$, **6b**$^+$, and **6a**$^+$ ($\Delta\delta_{P2,1}$ = 235 ppm in **2**$^+$). The correlation between these trends and the position of H_1 remains to be demonstrated. However, it is stimulating to observe that **4**$^+$−**6b**$^+$−**6a**$^+$ are also aligned in terms of decreasing π-basicity of the hydride-bearing platinum center Pt_2 or, more rigorously, of the metal which is the actual site of protonation in the corresponding series of their conjugated bases, i.e., $Pt_{1,2}$(**3**)−Pt_1(**5**)−Pt_2(**5**) (respectively defined as the Pt metals in **3** and the ones bonded to the phosphine or to CO in **5**). Indeed, in **3,** the common Pt$_2$(μ-PBu$^t_2$)$_2$ core is bonded to two σ-donor PBu$^t_2$H molecules, one of which is substituted by a π-acceptor CO molecule bonded to Pt_2 in **5**. It is expected[49] that the bond order between P_1 and H_1 in a three-center $Pt_2-H_1-P_1$ bond increases with the decrease of the π-back-donation from Pt_2 to the P−H antibonding orbital and, therefore, of the π-basicity of Pt_2 in the series $Pt_{1,2}$(**3**)−Pt_1(**5**)−Pt_2(**5**) (the strong M−H−P interaction found in complex **2** should be attributed to the lower basicity of palladium compared to platinum).[42]

Another point of considerable interest arises from the comparison of the IR spectra of the two isomers. The carbonyl absorption in the spectrum of **6b** (Nujol, KBr) was in fact found at 1990 (s, ν_{CO}) cm^{-1}, with a large bathochromic shift compared to **6a** (ν_{CO} = 2095 cm^{-1}). This may suggest that, although the *mean* formal oxidation state for the metal centers is +II, there is a substantial asymmetry in the charge distribution of the two isomers, the tricoordinated platinum being more reduced than the hydride-bearing center. Alternatively (or concurrently), the enhanced π-basicity of Pt_1 may be ascribed to the different geometries around Pt_1 and Pt_2 and/or to the influence of the hydride ligand bonded to Pt_2.

Mechanism of Isomerization. It is worth noting that a solution of **6a** in a well-dried solvent of low basicity, like $CHCl_3$ or CH_2Cl_2, remains unchanged after a week at room temperature but, after the addition of 5 μL of water, isomerization to **6b** occurs in a few hours. The isomerization **6a**−**6b** also takes place in anhydrous basic solvents (DME, acetone) and is slightly accelerated ($\tau_{1/2}$ ca. 1 h) by the addition of small quantities of a weak base like water. This evidence suggests that the isomerization proceeds through an intermolecular mechanism, with the external base acting as a proton "shuttle".[50]

In the presence of an excess of triflic acid, the kinetic isomer **6a** can be further protonated to a unique new product, which was identified as [Pt_2(μ-PBu$^t_2$)(μ-H)(CO)(PBu$^t_2$H)(η^2-PBu$^t_2$H)](CF$_3$SO$_3$)$_2$ (**7**) (eq 1) on the basis of its analytical and

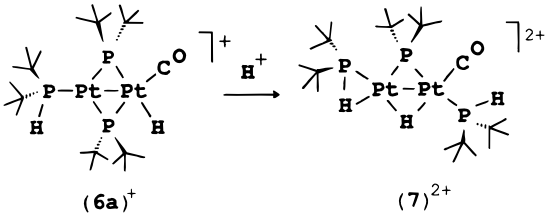

(1)

spectroscopic features. As will be shown later, complex **7** can be converted selectively and quantitatively into the thermodynamic hydride **6b**.

The ^{195}Pt{^{1}H} NMR spectrum of complex **7** (Figure 1) shows two signals at −5564 (ddd, $^1J_{Pt2P1}$ = 1300, $^1J_{Pt2P2}$ = 2010, $^2J_{Pt2P3}$ = 360 Hz, Pt_2) and −5205 ppm (ddd, $^1J_{Pt1P1}$ = 3300, $^1J_{Pt1P3}$ = 4060, $^2J_{Pt1P2}$ = 65 Hz, Pt_1), both flanked by weak satellites (isotopomer **D**, $^1J_{Pt1Pt2}$ = 1926 Hz). In the corresponding proton-coupled spectrum, the signal due to Pt_2 is further split by the coupling with the bridging hydride ($^1J_{Pt2H1}$ = 590 Hz), whereas

(49) Crabtree, R. H. *Angew. Chem., Int. Ed. Engl.* **1993**, *32*, 789.
(50) Quadrelli, E. A.; Kraatz, H.-B.; Poli, R. *Inorg. Chem.* **1996**, *35*, 5154.

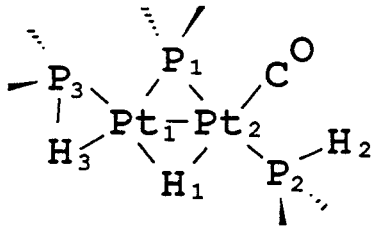

Isotop	Pt_1	Pt_2	%
A	-	-	43.8
B	195	-	22.4
C	-	195	22.4
D	195	195	11.4

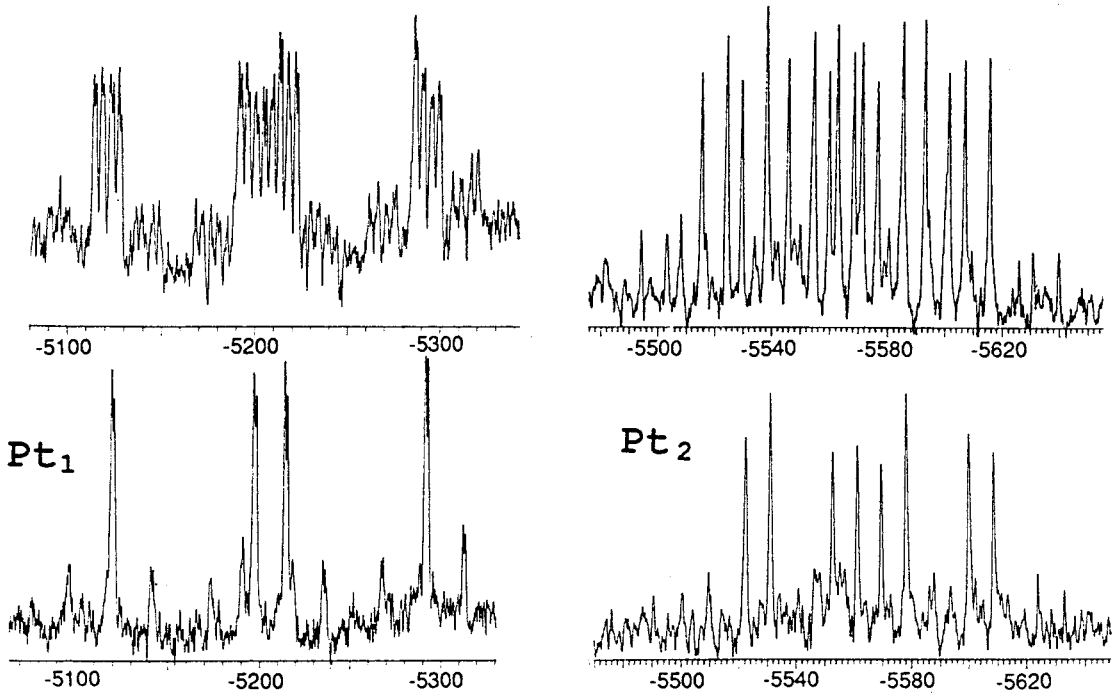

Figure 1. Proton-coupled (up) and proton-decoupled (below) ^{195}Pt NMR spectra ($CDCl_3$, 293 K) of **7**, with the atom-numbering and the isotopomer's composition scheme.

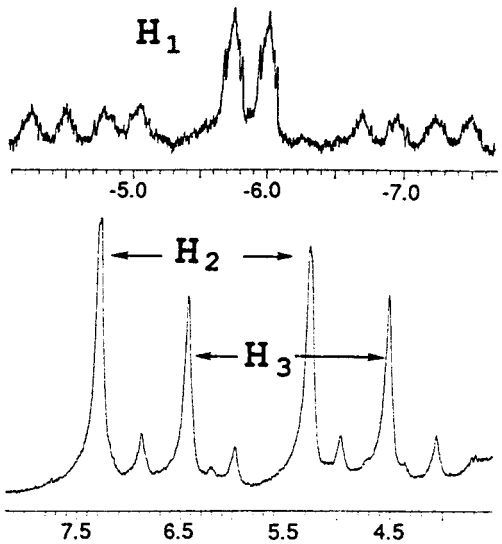

Figure 2. Hydride region (up) and P−H region (below) in the ^{1}H NMR spectrum ($CDCl_3$, 293 K) of **7**.

each line of the signal due to Pt_1 splits into four. Pt_1 is therefore coupled to *two* protons: the bridging hydride ($^1J_{Pt1H1}$ = 380 Hz) and the P−H proton H_3 ($^1J_{Pt1H3}$ = 180 Hz).

Both attributions are confirmed by the ^{1}H NMR spectrum (Figure 2). In fact, the bridging hydride H_1 gives a double multiplet at −5.9 ppm with the two expected different sets of satellites for the coupling with the two nonequivalent platinum centers. The two P−H protons resonate at 6.3 (H_2) and 5.5 (H_3) ppm as doublets, with the typical large $^1J_{PH}$ values (405 and 380 Hz, respectively). Only the signal for H_3 is flanked by ^{195}Pt satellites (J_{HPt} = 180 Hz). Since secondary phosphines terminally bonded in dinuclear platinum systems generally show values of $^2J_{PtH}$ 2 orders of magnitude smaller [less than line width (<2 Hz);[51−53] we found a small but observable value in a single case (complex **5**, $^2J_{PtH}$ = 27 Hz)[41]], such a large coupling constant strongly suggests that the secondary phosphine is engaged in a 3c−2e$^-$ interaction which brings H_3 in close contact to Pt_1.

The ^{31}P{^{1}H} NMR spectrum supports the presence of a Pt−H−P agostic interaction. It shows a low-field resonance (214 ppm) of the bridging phosphorus P_1 (dd, $^2J_{PP}$ = 175, 7.5 Hz, with ^{195}Pt satellites, $^1J_{P1Pt1}$ = 3300, $^1J_{P1Pt2}$ = 1300 Hz) and two high-field signals. These are centered at 27.5 ppm (d, $^2J_{P2P1}$ = 175 Hz; $^1J_{P2Pt2}$ = 2010, $^2J_{P2Pt1}$ = 65 Hz; P_2) and 27.0 ppm ($^2J_{P3P1}$ = 7.5 Hz; $^1J_{Pt1P3}$ = 4060, $^2J_{Pt2P3}$ = 360 Hz; P_3). The values of δ_{P2}, $^1J_{P2Pt2}$, and $^2J_{P1P2}$ clearly indicate that P_2 is bonded, trans to P_1, to a tetracoordinated platinum center (Pt_2)[47,48] and rule out structure **7b**. The large coupling of P_3 to the adjacent Pt_1 (4060 Hz) is close to the range observed for tricoordinated[47,48] phosphine complexes; however the values of δ_{P3} (27.0 ppm) and $^2J_{P3P1}$ (7.5 Hz) imply a reduction of the $P_3Pt_1P_1$ angle. These data rule out structure **7c** and agree with a Pt−H−P interaction

(51) Leoni, P.; Manetti, S.; Pasquali, M. *Inorg. Chem.* **1995**, *34*, 749.
(52) Kourkine, I. V.; Chapman, M. B.; Glueck, D. S.; Eichele, K.; Wasylishen, R. E.; Yap, G. P. A.; Liable-Sands, L. M.; Rheingold, A. L. *Inorg. Chem.* **1996**, *35*, 1478.
(53) Blum. T.; Braunstein, P. *Organometallics* **1989**, *8*, 2497.

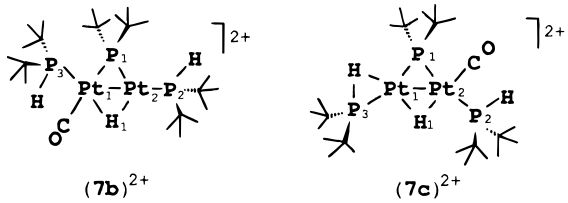

pushing P_3 toward the phosphide [note that the coordination of other weak ligands is ruled out by the constancy of the whole coupling constant pattern upon variations of the counterion ($CF_3SO_3^-$, BF_4^-; see the Experimental Section) or the solvent ($CDCl_3$, CD_2Cl_2, DME)]. The carbonyl stretching absorption was found at 2103 cm^{-1} in the IR spectrum (Nujol, KBr).

Complex **7** is the first non-palladium derivative showing an M−H−P 3c−2e$^-$ interaction. Up to now, this type of interaction has only been observed in the palladium complex **2**[40] and its strictly related derivatives.[54,55] By comparing the two types of interactions, we note that in the palladium case there was a much higher reduction of the P−H bond order, as suggested by the values of $\delta_{H(PH)}$ (around 0 ppm) and $^1J_{PH}$ (136−161 Hz).[54,55] In fact, although E−H−M interactions *often* show reduced $^1J_{EH}$ coupling constants, an upfield shift of δ_H, and a substantial lengthening of the E−H bond,[56,57] numerous exceptions to this behavior have been reported.[58−65] For example, the values of $^1J_{HD}$ for well-established M(η^2-HD) complexes are spread over a large interval (11−34 Hz) between the values observed for free HD (43.2 Hz) and for M(H)(D) derivatives (<3 Hz);[58] moreover, several reports show that C−H−M interactions can leave $^1J_{CH}$ practically *unchanged* [59−63] and also cause *high-field* shifts.[59,60] On the other hand, the difference observed between the palladium and the platinum systems can be the result of the different electronic distributions, or ring strain, between the β-agostic Pd···H−P−Pd unit and the α-agostic Pt···H−P unit.[65] Furthermore, the reduction of the P−H bond order is expected to grow with the π-back-donation into the antibonding σ^* orbital of the PH bond,[49] and a much higher π-basicity is expected for the palladium fragment (Pd_2^I, monocation) compared to the platinum fragment (Pt_2^{II}, dication).

The mechanism of the reaction of eq 1 may be described as the attack of a proton on one of the metal centers, followed by the formation of a P−H bond between the phosphide and hydride ligands (eq 2a).

Alternatively, the reaction could proceed through the direct protonation of one of the bridging nuclei, followed by the displacement of the hydride from the terminal to the bridging position (eq 2b).

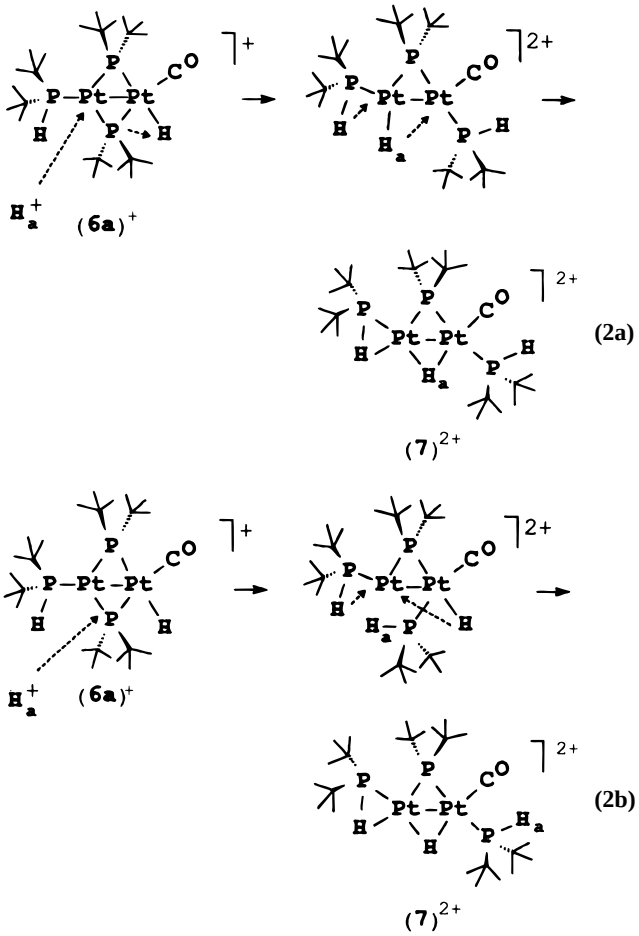

Which of the two is closer to the real mechanism was clearly indicated by the results of the following experiment. A CH_2Cl_2 solution of the neutral carbonyl **5** was reacted first with 1 equiv of CF_3SO_3H and then, when the $^{31}P\{^1H\}$ NMR spectra confirmed that the formation of **6a** was quantitative, with 1 equiv of CF_3SO_3D. The reaction afforded selectively and quantitatively the deuteride-bridged complex [Pt$_2$(μ-PBu$^t_2$)(μ-D)(CO)(PBu$^t_2$H)(η^2-PBu$^t_2$H)](CF_3SO_3)$_2$ (**7-D**), clearly supporting the path shown in eq 2a. The site of deuteration in **7-D** was clearly shown by its ^1H NMR spectrum, which exhibits resonances due to the P−H protons of the two types of PBu$^t_2$H molecules and those assigned to the *tert*-butyl protons in a 1/1/54 integral ratio. Only a very small residual signal, resulting from the small percent of nondeuterated acid in the commercial sample of CF_3SO_3D, was found at −5.9 ppm. The $^{31}P\{^1H\}$ NMR spectrum was identical to the one exhibited by **7**, whereas both signals in the ^{195}Pt NMR spectrum showed a greater complexity due to the Pt−D couplings.

Complex **7** remained unchanged in anhydrous $CDCl_3$ or CH_2Cl_2 (1 week at room temperature) or in the presence of an excess of CF_3SO_3H. It was instead converted (6 h) to **6b** when dissolved in a basic solvent like acetone or DME. Upon the addition of a stoichiometric amount of a stronger base like water to a stable chloroform solution, the conversion is instantaneous ($^{31}P\{^1H\}$ NMR) (eq 3).

$$\mathbf{7}^{2+} + H_2O \rightarrow \mathbf{6b}^+ + H_3O^+ \qquad (3)$$

(54) Leoni, P.; Pasquali, M.; Sommovigo, M.; Albinati, A.; Lianza, F.; Pregosin, P. S.; Rüegger, H. *Organometallics* **1994**, *13*, 4017.
(55) Leoni, P.; Pieri, G.; Pasquali, M. *J. Chem. Soc., Dalton Trans.* **1998**, 657.
(56) Brookhart, M.; Green, M. L. H.; Wong, L.-L. *Prog. Inorg. Chem.* **1988**, *36*, 1.
(57) Crabtree, R. H.; Hamilton, D. G. *Adv. Organomet. Chem.* **1988**, *28*, 299.
(58) Heynekey, D. M.; Oldham, W. J., Jr. *Chem. Rev.* **1993**, *93*, 913.
(59) Albinati, A.; Arz, C.; Pregosin, P. S. *Inorg. Chem.* **1987**, *26*, 508.
(60) Albinati, A.; Pregosin, P. S.; Wombacher, F. *Inorg. Chem.* **1990**, *29*, 1812
(61) Deeming, A. J.; Rothwell, I. P.; Hursthouse, M. B.; Malik, K. M. A. *J. Chem. Soc., Dalton Trans.* **1980**, 1974.
(62) Neve, F.; Ghedini, M.; Crispini, A. *Organometallics* **1992**, *11*, 3324.
(63) Schwartz, D. J.; Ball, G. E.; Andersen, R. A. *J. Am. Chem. Soc.* **1995**, *117*, 6027.
(64) Viñas, C.; Nuñez, R.; Teixidor, F.; Kivekäs, R.; Sillanpää, R. *Organometallics* **1996**, *15*, 3850.
(65) Scherer, W.; Priermeier, T.; Haaland, A.; Volden, H. V.; McGrady, G. S.; Downs, A. J.; Boese, R.; Bläser, D. *Organometallics* **1998**, *17*, 4406.
(66) Leoni, P.; Chiaradonna, G.; Pasquali, M.; Marchetti, F.; Fortunelli, A.; Germano, G. *Inorg. Chim. Acta* **1997**, *264*, 185.

Two alternative mechanisms can be postulated for this reaction, the former assuming that the base deprotonates **7** to **6a** and then converts the latter to **6b**.

Alternatively, **7** can be deprotonated to yield *directly* **6b**, as shown in eq 4.

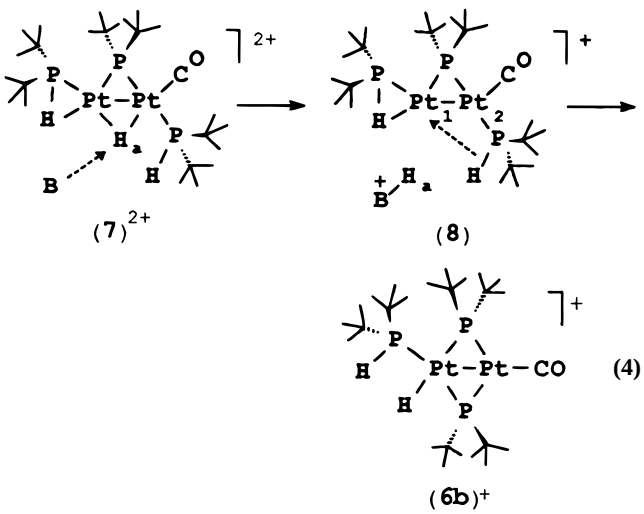

Since the conversion **7**−**6b** promoted by the addition of water is immediate, whereas the isomerization **6a**−**6b** performed under the same conditions occurred in some hours, and since **6a** was not observed in the early steps of the conversion, the direct mechanism shown in eq 4 seems preferable. This is the microscopic reverse of the formation of **7** (eq 2a) up to the withdrawal of the bridging hydride yielding the intermediate **8**. The latter can evolve through the oxidative addition of the P−H bond of the PBu^t_2H molecule bonded to Pt_2, which would regenerate **6a** by occurring on Pt_2 and would form **6b** by occurring on Pt_1. The approach of the P−H bond to Pt_1 in **8** is much less hindered compared to the approach of CF_3SO_3H to the corresponding metal center of complex **5**, which bears a PBu^t_2H ligand and two μ-PBu^t_2 ligands. The reduction of the steric congestion around Pt_1 in **8** is further assisted by the Pt−H−P agostic interaction undertaken by the other secondary phosphine, which keeps its *tert*-butyls on the opposite side of the approaching P−H bond. The oxidative addition occurs therefore on the more basic center Pt_1, and **6b** is selectively formed.

Theoretical Analysis. We have performed ab initio calculations on models of complexes **6a**,**b** to determine for these molecules the minimum-energy structures, the bonding situations, the main vibrational frequencies, and the energy differences among the different species. The compounds which will be considered in the following are "model" ones because (a) their structures have been optimized in the gas phase, without introducing any solid-state or solvation effect, and (b) the *tert*-butyl substituents have been replaced with methyl groups (with their hydrogen atoms placed along the C−C bonds of the *tert*-butyl groups at 65% of the C−C distance). We refer to a previous paper[66] showing that this replacement does not substantially affect the electronic properties of the "core" region. For the sake of simplicity in the following, we will not distinguish among **5**, $\mathbf{6a}^+$, and $\mathbf{6b}^+$ and their model analogues.

Geometry Optimization of 5. For molecule **5**, the crystallographic structure is available.[41] It can thus be interesting to optimize its geometry by using different theoretical methods and to compare the corresponding results. To this aim, we have selected three methods: the standard Hartree−Fock (HF) approach and two density functional (DF) approaches, utilizing (a) the exchange functional proposed by Becke[67] and the correlation functional proposed by Lee, Yang, and Parr[68] (BLYP approach) and (b) a "hybrid" approach which mixes the HF exchange functional with the DF one[69] (B3LYP approach). All geometrical parameters have been left free in the optimizations. In Table 2, we report the most relevant interatomic distances obtained through ab initio calculations on **5** using these theoretical approaches.

First of all, it can be noted that the theoretically derived distances are always larger than the experimental ones. This may be due to the lack of solid-state effects in the ab initio simulations or—much more importantly—to the incomplete inclusion of relativistic effects. A full account of these effects would strengthen all the bonds involving a platinum atom and bring the ab initio distances into closer agreement with the experimental ones.[70]

From an inspection of Table 2, it can also be clearly seen that no method is apparently superior to the others. The HF approach gives Pt−P(phosphide) and Pt−Pt distances in better agreement with experiment than the BLYP approach. But it also predicts $Pt-P_{term}$ and Pt−CO distances larger than the experimental ones with respect to the BLYP values. The B3LYP values are often between the HF and BLYP values. This is in contrast with the current finding that the B3LYP method improves over the BLYP method the accuracy of structural predictions. However, we decided to choose the B3LYP approach as a compromise in which all interatomic distances are more or less equally overestimated: the calculations discussed in the following have thus been performed by using this method. It is interesting to note, in passing, that at the theoretical level the Pt−P(phosphide) bonds adjacent to the CO ligand are longer than those on the opposite side. This is likely due to the strong bonding characteristics of the CO ligand, which engages the electrons of the Pt atom and weakens the neighboring Pt−P bonds. The lack of this effect at the crystallographic level is probably due to steric and packing effects. However, it can be observed that NMR solution data[41] for **5** are in agreement with the theoretical predictions ($^1J_{P1,2Pt1} = 2623$, larger than $^1J_{P1,2Pt2} = 2431$ Hz).

Fully Optimized Structures of $\mathbf{6a}^+$ and $\mathbf{6b}^+$. The B3LYP approach was then used to derive the fully optimized structures of $\mathbf{6a}^+$ and $\mathbf{6b}^+$ (Table 2).

The first manifest point from an analysis of these results is that H_1 is bonded only to Pt_2 in both $\mathbf{6a}^+$ and $\mathbf{6b}^+$. In other words, there is no sign of an agostic Pt−H−P interaction. In particular, the short Pt_2-H_1 distance (1.61−1.62 Å) and the long $P_1\cdots H_1$ distance (2.58−2.62 Å) exclude such a possibility. In fact, these are close enough to the values found for $\mathbf{4}^+$ (1.64−1.67 and 2.11−2.19 Å, respectively) and far from those of the Pd analogue $\mathbf{2}^+$ (1.79 and 1.55−1.67 Å, respectively) in which a Pd−H−P agostic interaction was instead found.

A further analysis of the results (Table 2) allows one to point out the main effects of protonation on the structure of **5**, which are as follows:

(1) In contrast to what is exhibited by $\mathbf{4}^+$, here protonation seems to weaken (lengthen) the Pt−Pt bond. This may be due to the presence of the π-acceptor CO ligand, which drags the excess of charge drawn from the other ligands and prevents it from being accumulated in the Pt−Pt bond.

(67) Becke, A. D. *Phys. Rev. B* **1988**, *38*, 3098.
(68) Lee, C.; Yang, W.; Parr, R. G. *Phys. Rev. B* **1988**, *37*, 785.
(69) Becke, A. D. *J. Chem. Phys.* **1993**, *98*, 5648.
(70) See, for example: Fantucci, P.; Polezzo, S.; Sironi, M.; Bencini, A. *J. Chem. Soc., Dalton Trans.*,**1995**, 4121.

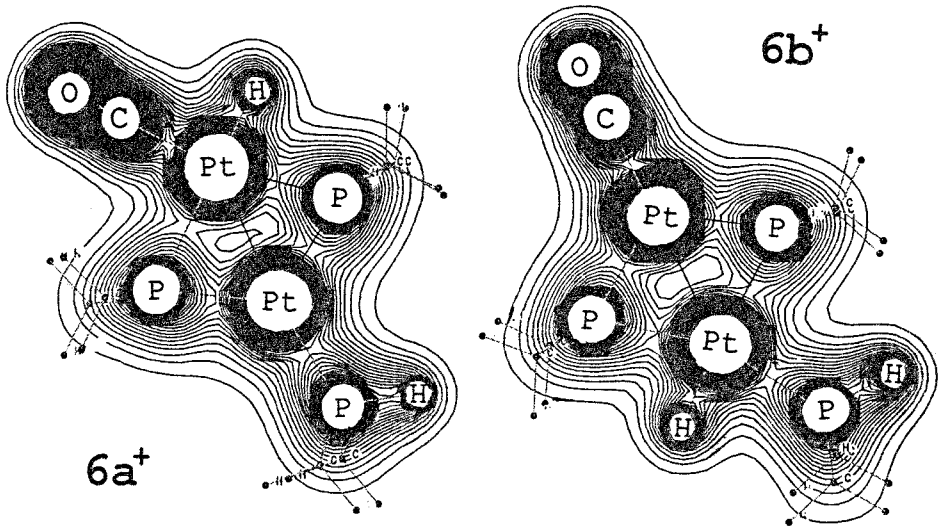

Figure 3. Contour plots of the total electron density (in au) of the cations **6a**$^+$ and **6b**$^+$ in the P−H−Pt−CO plane. A maximum along directions roughly orthogonal to a line connecting two nuclei is a characteristic feature of a chemical bond. The circle at the center of the two molecules encloses a (3,1) and two (3,3) critical points. Isodensity lines were plotted every 0.01 unit.

(2) A strong trans influence of the hydride ligand is apparent. The Pt$_2$−P$_2$ bond length increases (by 2.59 Å in **6a**$^+$, i.e., 0.2−0.3 Å longer than the other Pt−P distances in **5** and **6a**$^+$). The trans-hydride influence may be combined with a cis-carbonyl influence, since the lengthening of the Pt$_2$−P$_2$ bond is much more pronounced in **6a**$^+$ than in **6b**$^+$. As a consequence of these effects, the electron distribution in cation **6a**$^+$ is strongly asymmetrical with respect to that in **6b**$^+$; this is also apparent from the plots of the total electron density in the Pt−Pt−P plane shown in Figure 3 for **6a**$^+$ and **6b**$^+$.

(3) The Pt−CO bond length increases and the C−O distance decreases in the series **5**, **6b**$^+$, and **6a**$^+$, which corresponds to the observed trend of ν_{CO} values (1956, 1990, and 2095 cm^{-1}, respectively). The large ν_{CO} shift from **6b**$^+$ to **6a**$^+$ may be due to the presence of the hydride which engages part of the Pt$_2$ d electrons, making them less available for the Pt−CO π-back-bonding interaction in **6a**$^+$. A vicinal hydride ligand influence can also be invoked to explain the lengthening of the Pt−P$_{term}$ bond in **6b**$^+$.

Constrained Optimizations of Structures 6a$^+$ and 6b$^+$. One may wonder whether other effects might modify the previous conclusions concerning the absence of an agostic interaction in the protonated species. In particular, one may imagine that steric effects can impose particular geometrical constraints that may favor the rise of a Pt−H−P agostic interaction. To check this possibility, B3LYP calculations were performed again on **6a**$^+$ and **6b**$^+$, in which the overall skeleton was fixed at the experimental structure of **5** and the only available degrees of freedom were associated with the motion of H$_1$. The new optimized Pt$_2$−H$_1$ and P$_1$−H$_1$ distances are 1.770 and 1.592 Å, respectively, for **6a**$^+$ and 1.807 and 1.594 Å, respectively, for **6b**$^+$, with the hydrogen atom remaining approximately in the Pt$_1$Pt$_2$P$_2$ plane. It is thus clear that in this case a three-center Pt−H−P bond is formed for both **6a**$^+$ and **6b**$^+$ (this is also confirmed by the analysis of the electron density; see Figure 4).

As clearly apparent from Figure 4, the three-center character of the bonding is stronger in **6a**$^+$ than in **6b**$^+$, therefore confirming the qualitative prediction that it should grow in the series **4**$^+$−**6b**$^+$−**6a**$^+$ (we recall that under similar conditions a three-center bond is not formed in **4**$^+$).[42]

The fact that an agostic bond is not formed when the overall skeleton is left free in the optimization process is particularly interesting, since it shows that particular geometrical rearrangements may create the premises for the formation of a Pt−H−P agostic interaction. A low-energy configuration with an agostic Pt−H−P interaction is therefore potentially available for these compounds and may have an appreciable influence on their reactivity. For example, it can represent the first step in the protonation process. Or it can operate in the formation of a P(phosphide)−H bond, either as a stable configuration or as a transition state, any time that the hydride ligand is pushed toward the adjacent P(phosphide) by the incoming of a new ligand; the mechanism of the protonation of **6a**, yielding complex **7** (eq 2a above), gives the first experimental evidence of this behavior.

Analysis of the Charge Distribution. We have suggested above that Pt$_{1,2}$(**3**)−Pt$_1$(**5**)−Pt$_2$(**5**) can be aligned in order of decreasing π-basicity. This assumption may be compared with an analysis of the charge density on complexes **3** and **5**. Since the Mulliken analysis employed in our previous works[42,66] is not reliable in conjunction with the large basis set utilized here, we performed further calculations at the optimized geometries by using the smaller double-ζ basis set of refs 42 and 66. We found the following Mulliken gross charges (Q) in **5**: Q(Pt$_1$) = −0.35 and Q(Pt$_2$) = −0.08 (at the BLYP level, but very similar results were found at the B3LYP level), with the phosphine-bearing platinum becoming more electron-rich than the CO-bonded platinum. Since the two Pt atoms in **3** gave Q = −0.44,[42] the expected decrease of the π-basicity of the Pt atom in the series Pt$_{1,2}$(**3**)−Pt$_1$(**5**)−Pt$_2$(**5**) is fairly confirmed. This trend can be correlated with the increase of the three-center character of the Pt$_2$−H$_1$−P$_2$ bond in the series **4**$^+$−**6b**$^+$−**6a**$^+$ found in the constrained optimizations. However, it does not correlate with the position of H$_1$ in the full optimizations (see above). The peculiar asymmetric electron distribution found in cations **6b**$^+$ and (especially) **6a**$^+$ (point 2 above), rather than the P$_2$···H$_1$ distance, may provide an alternative explanation for the observed trends in the $\Delta\delta_{P1,2}$ and δ_{H1} values.

Complementary results have been obtained through a Bader topological analysis.[71] We performed it at the crudest possible level, by simply locating the critical points of the total electron density, and found all the expected ones. In particular, we found

(71) Bader, R. F. W. *Atoms in Molecules: A Quantum Theory*; Oxford University Press: Oxford, U.K., 1990.

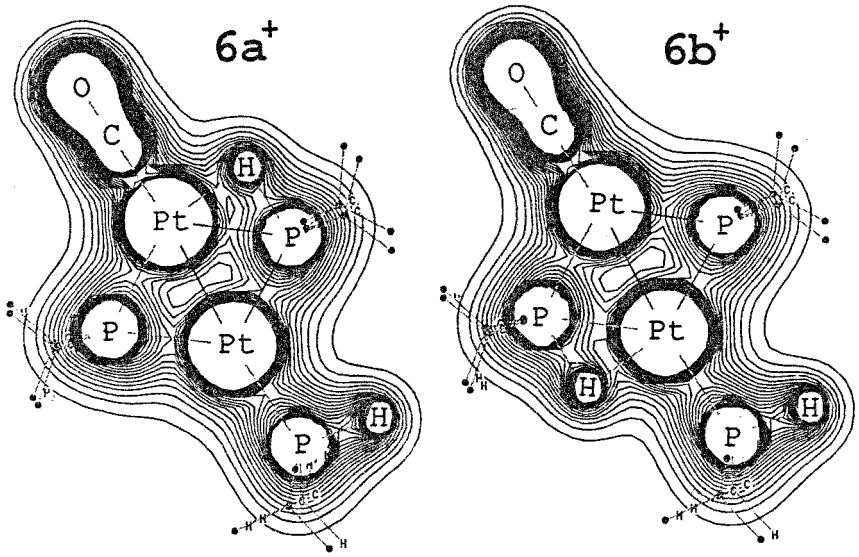

Figure 4. Contour plots of the total electron density (in au) of the cations **6a**$^+$ and **6b**$^+$ in the P−H−Pt−CO plane, obtained by freezing the overall skeleton to the structure of **5** and optimizing the position of the additional H atom only. The (3,3) critical points corresponding to the three-center Pt−H−P bonds are clearly visible. The density holes around the Pt nuclei are due to the use of pseudopotentials, which allow neglecting the core electrons in the calculations. Isodensity lines were plotted every 0.01 unit.

Table 3. Calculated Total Electron Density for Selected Interatomic Regions[a]

	Pt_1-Pt_2	Pt_1-P_1	Pt_1-P_2	Pt_2-P_1	Pt_2-P_2	$Pt-P_{term}$	Pt−C	C−O	Pt_2-H_1
5	0.061	0.093	0.090	0.088	0.085	0.104	0.157	0.484	
6a$^+$	0.049	0.103	0.099	0.089	0.065	0.108	0.143	0.490	0.127
6b$^+$	0.055	0.098	0.096	0.090	0.081	0.098	0.152	0.487	0.129

[a] Values in au of the total electron density at the critical points for the model compounds corresponding to **5**, **6a**$^+$, and **6b**$^+$, as derived from B3LYP calculations.

the (3,1) Pt−P, Pt−H, Pt−C, and C−O critical points, plus a (3,1) critical point approximately at the center of the $Pt_2(\mu\text{-}P)_2$ square and two (3,3) critical points connecting it with the P(phosphide) atoms. In Table 3, the values of the total electron density at these points are reported. An analysis of Table 3 leads to the same conclusions (1)−(3) derived above from an analysis of the structural data: (1) the Pt−Pt bond weakening due to protonation; (2) the strong hydride ligand trans influence; (3) the weakening of the Pt−CO bond in the sequence **5** > **6b**$^+$ > **6a**$^+$, with the parallel strengthening of the C−O bond, as well as the weakening of the $Pt-P_{term}$ bond in **6b**$^+$.

Energetics and Vibrational Frequencies. To conclude, let us analyze the energetics and the main vibrational frequencies of the compounds here considered. The total energies of **5**, **6a**$^+$, and **6b**$^+$ at the optimized structures derived at the B3LYP level are −1616.418 934, −1616.806 083, and −1616.812 432 au, respectively (the core energy is missing due to the use of pseudopotentials on the platinum atoms). It can be seen that **6b**$^+$ is more stable than **6a**$^+$ by ∼4 kcal/mol, which fully agrees with the experimental observation that **6a**$^+$ is formed under kinetic control but isomerizes quantitatively to **6b**$^+$.

The vibrational frequencies of the Pt−H, C−O, and P−H stretchings have also been evaluated in an approximate way by considering only the selected modes and freezing all the remaining degrees of freedom. The results of these calculations are reported in Table 4, together with the experimental results. It can be seen that the experimental trends (even though not as accurately as the absolute values) are fairly reproduced by the ab initio calculations, thus furnishing further support to the previous theoretical analysis and interpretation of experimental data.

Table 4. Vibrational Frequencies[a]

	ν_{CO}	ν_{PH}	ν_{Pt-H}
5	2067	2374	···
	(1956)	(2277)	(···)
6a$^+$	2183	2442	2101
	(2095)	(2335)	(2043)
6b$^+$	2144	2449	2064
	(1990)	(2303)	(2027)

[a] Theoretical values at the B3LYP level. Experimental values in parentheses, taken from ref 41 and the present work. All the quantities are given in cm $^{-1}$.

Conclusions

This paper shows that the protonation of complex **5** occurs with the formation of the terminal hydride **6a** under kinetic control. Complex **6a** can be isolated as a pure solid and is stable even in solutions of nonbasic media. However, **6a** is converted cleanly and quantitatively into the thermodynamic isomer **6b**, with the hydride on the more basic and more hindered metal center, in the presence of weak bases which "shuttle" the proton from the kinetic to the thermodynamic site. A theoretical investigation of gas-phase models of complexes **5**, **6a**, and **6b** estimates that **6b** is ca. 4 kcal/mol more stable than **6a** and confirms that both should be considered as terminal hydrides. It however suggests that a small distortion of the geometrical features of the skeleton, pushing the hydride closer to the P(phosphide) nucleus, can induce the formation of a three-center Pt−H−P bond. This was experimentally confirmed when we studyied the reaction of **6a** with a strong acid. Complex **7**, which forms under these conditions, was in fact shown to build through the formation of a P−H bond from the hydride and the adjacent P(phosphide) induced by the approach of the acid to a metal center. The interesting dicationic derivative **7**, which exhibits

an unprecedented Pt−H−P agostic interaction, can again be isolated pure or converted into **6b**. The presence of an agostic interaction in **7** is suggested by the uncommonly large value of the coupling between the P−H proton and the adjacent platinum center (J_{PtH} = 180 Hz) and by the severe distortion of the geometry around the metal ($^2J_{P3P1}$ = 7.5 Hz); the high-field shift of δ_H and the reduction of $^1J_{PH}$ are relatively small, suggesting a small reduction of the P−H bond order.

Since **6a**, **6b**, and **7** can be isolated as pure compounds in high yields and each of them is stable under the appropriate experimental conditions, their reactivities can be investigated separately. Differences and analogies between the chemical behavior of the two isomeric terminal hydrides **6a** and **6b** will be communicated in a future paper.

Experimental Section

General Data. If not differently specified, all reactions were carried out under an N_2 atmosphere, by using standard Schlenk techniques. $(Bu^t_2HP)Pt(\mu\text{-}PBu^t_2)_2Pt(CO)$ (**5**) was prepared as previously described.[41]

Solvents were dried by conventional methods and distilled under nitrogen prior to use. IR spectra (Nujol mulls, KBr) were recorded with a Perkin-Elmer Fourier transform IR 1725X spectrophotometer. NMR spectra were recorded with a Varian Gemini 200 BB instrument; frequencies are referenced to Me_4Si (^{1}H), 85% H_3PO_4 (^{31}P), and H_2PtCl_6 (^{195}Pt).

Preparation of 6a. A red solution of complex **5** (220 mg, 0.258 mmol) in dichloromethane (15 mL) turned yellow within the time of mixing with an equimolar amount of CF_3SO_3H. The solution was kept 15 min at room temperature, and a sample was analyzed by $^{31}P\{^1H\}$ NMR spectroscopy, which exhibited the complete consumption of complex **5** and the resonances of **6a** (Tab. 1) as the unique P-containing product. Most of the solvent was evaporated, after which Et_2O (20 mL) was added with vigorous stirring; a yellow powder precipitated and was filtered off, washed with Et_2O (5 mL), and dried under vacuum (156 mg, 60.2%). Anal. Calcd for $C_{26}H_{56}F_3O_4P_3Pt_2S$: C, 31.1; H, 5.62. Found: C, 30.9; H, 5.65. IR (Nujol, KBr): 2335 (w, ν_{PH}), 2095 (s, ν_{CO}), 2043 (w, ν_{PtH}), 1262, 1151, 1033, 639 cm^{-1} (uncoordinated triflate).[72] See Table 1 for NMR parameters.

Preparation of 6b. A red solution of complex **5** (180 mg, 0.210 mmol) in dichloromethane (10 mL) turned yellow within the time of mixing with an equimolar amount of CF_3SO_3H and 4 μL (0.222 mmol) of H_2O. The solution was kept overnight at room temperature, and a sample was analyzed by $^{31}P\{^1H\}$ NMR spectroscopy, which exhibited the complete consumption of complex **5** and the resonances of **6b** (Table 1) as the unique P-containing product. Most of the solvent was evaporated, after which Et_2O (15 mL) was added with vigorous stirring; a yellow powder precipitated and was filtered off, washed with Et_2O (5 mL), and dried under vacuum (120 mg, 56.9%). Anal. Calcd for $C_{26}H_{56}F_3O_4P_3Pt_2S$: C, 31.1; H, 5.62. Found: C, 31.5; H, 5.90. IR (Nujol, KBr): 2303 (w, ν_{PH}), 2027 (w, ν_{PtH}), 1990 (s, ν_{CO}), 1265, 1149, 1031, 637 cm^{-1} (uncoordinated triflate).[72] See Table 1 for NMR parameters.

Preparation of 7. A red solution of complex **5** (320 mg, 0.274 mmol) in dichloromethane (14 mL) turned yellow within the time of mixing with CF_3SO_3H (100 μL, 1.145 mmol). The solution was kept 2 d at room temperature, and a sample was analyzed by $^{31}P\{^1H\}$ NMR spectroscopy, which exhibited the complete consumption of complex **5** and the resonances of **7** (Table 1) as the unique P-containing product. Most of the solvent was evaporated, after which Et_2O (10 mL) was added with vigorous stirring; a colorless microcrystalline solid precipitated and was filtered off, washed with Et_2O (5 mL), and dried under vacuum (185 mg, 58.5%). Anal. Calcd for $C_{27}H_{57}F_6O_7P_3Pt_2S_2$: C, 28.1; H, 4.97. Found: C, 28.3; H, 4.94. IR (Nujol, KBr): 2364 (w, ν_{PH}), 2103 (s, ν_{CO}), 1263, 1150, 1030, 638 cm^{-1} (uncoordinated triflate).[72] See Table 1 for NMR parameters. The same complex was obtained by reacting complex **6a** with an excess of CF_3SO_3H. Identical solution NMR (^{1}H, ^{31}P, ^{195}Pt) spectra were observed when $HBF_4{\cdot}Et_2O$ was used in place of triflic acid.

Preparation of 7-D. A well-dried NMR tube was charged with complex **5** (20 mg, 0.023 mmol), $CDCl_3$ (0.4 mL), and CF_3SO_3H (2 μL, 0.023 mmol). As soon as the $^{31}P\{^1H\}$ NMR spectrum confirmed the complete conversion of **5** into **6a**, CF_3SO_3D (2 μL, 0.023 mmol) was added. After 12 h at room temperature, the $^{31}P\{^1H\}$, ^{1}H, and $^{195}Pt\{^1H\}$ NMR spectra confirmed the complete conversion of **6a** into **7-D**. See results and discussion for NMR parameters.

Conversion of 7 into 6b. Complex **7** (25 mg, 0.021 mmol) was dissolved in $CDCl_3$ (0.5 mL) in a well-dried NMR tube. After 5 h at room temperature, the $^{31}P\{^1H\}$ NMR spectrum was still showing only the resonances of complex **7**. The addition of 0.5 μL of H_2O immediately caused the disappearance of these signals and the appearance of the resonances due to **6b**.

In a separate experiment, 15 mg of complex **7** was dissolved in acetone-d_6 (0.4 mL). The $^{31}P\{^1H\}$ NMR spectra showed the slow (6 h) complete conversion of **7** into **6b**.

Computational Details. The ab initio Hartree−Fock and density functional calculations were performed with the Gaussian 94[73] set of programs. All the calculations utilize a triple-ζ-valence-plus-polarization basis set for the platinum atom[74] (including the pseudopotential proposed in the literature[75]) and the standard double-ζ-plus-polarization 6-31G** basis set for the other atoms.[76] This basis set uses pseudopotentials and incorporates spin−orbit averaged relativistic effects for the Pt atom. Despite the incomplete account of spin−orbit effects and the lack of Darwin and mass-polarization relativistic corrections in the pseudopotentials, the present computational approach usually describes in a reasonable way the energetics of the Pt−H, Pt−P and P−H bonds. The Bader population analysis[71]—not supported by Gaussian 94—was performed at the simplest possible level by locating the critical points of the total electron density through direct inspection of plots in the proper plane.

Acknowledgment. The Consiglio Nazionale delle Ricerche (CNR) and the Ministero dell'Università e della Ricerca Scientifica e Tecnologica (MURST) are gratefully acknowledged for financial support.

IC9903228

(72) Johnstone, D. H.; Shriver, D. F. *Inorg. Chem.* **1993**, *32*, 1045.

(73) Frisch, M. J.; Trucks, G. W.; Schlegel, H. B.; Gill, P. M. W.; Johnson, B. G.; Robb, M. A.; Cheeseman, J. R.; Keith, T.; Petersson, G. A.; Montgomery, J. A.; Raghavachari, K.; Al-Laham, M. A.; Zakrzewski, V. G.; Ortiz, J. V.; Foresman, J. B.; Cioslowski, J.; Stefanov, B. B.; Nanayakkara, A.; Challacombe, M.; Peng, C. Y.; Ayala, P. Y.; Chen, W.; Wong, M. W.; Andres, J. L.; Replogle, E. S.; Gomperts, R.; Martin, R. L.; Fox, D. J.; Binkley, J. S.; Defrees, D. J.; Baker, J.; Stewart, J. P.; Head-Gordon, M.; Gonzalez, C.; Pople, J. A. *Gaussian 94*, Revisions B.3 and D.4; Gaussian, Inc.: Pittsburgh, PA, 1995.

(74) Schafer, A.; Huber, C.; Ahlrichs, R. *J. Chem. Phys.* **1994**, *100*, 5829.

(75) Andrae, D.; Haeussermann, U.; Dolg, M.; Stoll, H.; Preuss, H. *Theor. Chim. Acta* **1990**, *77*, 123.

(76) Hehre, W. J.; Ditchfield, R.; Pople, J. A. *J. Chem. Phys.* **1972**, *56*, 2257.